Article

Optimal Compartmentalization Strategies for Metabolic Microcompartments

Florian Hinzpeter,[1,*] Ulrich Gerland,[1] and Filipe Tostevin[1]
[1]Department of Physics, Technische Universität München, Garching, Germany

ABSTRACT   Intracellular compartmentalization of cooperating enzymes is a strategy that is frequently used by cells. Segregation of enzymes that catalyze sequential reactions can alleviate challenges such as toxic pathway intermediates, competing metabolic reactions, and slow reaction rates. Inspired by nature, synthetic biologists also seek to encapsulate engineered metabolic pathways within vesicles or proteinaceous shells to enhance the yield of industrially and pharmaceutically useful products. Although enzymatic compartments have been extensively studied experimentally, a quantitative understanding of the underlying design principles is still lacking. Here, we study theoretically how the size and enzymatic composition of compartments should be chosen so as to maximize the productivity of a model metabolic pathway. We find that maximizing productivity requires compartments larger than a certain critical size. The enzyme density within each compartment should be tuned according to a power-law scaling in the compartment size. We explain these observations using an analytically solvable, well-mixed approximation. We also investigate the qualitatively different compartmentalization strategies that emerge in parameter regimes where this approximation breaks down. Our results suggest that the different sizes and enzyme packings of α- and β-carboxysomes each constitute an optimal compartmentalization strategy given the properties of their respective protein shells.

INTRODUCTION

Metabolic processes in living organisms are highly regulated and in many cases also coordinated in space. For instance, collaborating enzymes are often organized into multi-enzyme complexes and compartments (1–4). Such spatial organization is believed to have evolved as a strategy to overcome certain challenges inherent to intracellular metabolism. Intermediate products of a pathway can be toxic for the cell or poorly retained by the cell membrane, or they can cause undesired side reactions (5,6). Furthermore, enzymes can be inefficient or have a low specificity for the desired reaction (7). Spatial confinement of reactants can alleviate both of these limitations.

Metabolic reactions can be organized in space through different mechanisms and on different scales, from individual molecules to populations of cells (8). On a molecular level, direct interactions between enzymes, or between enzymes and scaffold proteins, enables "metabolic channeling" of intermediate products from one enzyme to the next, eliminating the need for diffusive transport over long distances (9,10). Additionally, quantitative modeling has

shown that colocalizing enzymes in space can enhance the processing of pathway intermediates, even in the absence of direct enzyme-enzyme interactions (11–13). On the cellular scale, loss of intermediate products and unwanted side reactions can be reduced by encapsulating enzymatic pathways within subcellular compartments (14). At the level of populations of cells, microbial consortia can be structured such that each species is able to efficiently exploit the metabolic products of the others (8).

Here, we focus on metabolic reactions taking place within subcellular microcompartments. The segregation of metabolic processes into organelles is a hallmark of eukaryotic cells. A well-studied example of such an organelle is the peroxisome that encloses enzymes that produce and consume hydrogen peroxide, which can be highly toxic (15). The discovery of bacterial microcompartments (BMCs) demonstrated that compartmentalization is also used by prokaryotes (16,17). In contrast to the lipid membranes that typically define eukaryotic organelles, BMCs have protein shells reminiscent of viral capsids. Small pores in the shell allow metabolites, but not enzymes, to pass into and out of the compartment (18).

The best-studied BMC, the carboxysome, is a key element of so-called "carbon-concentrating mechanisms" that are crucial for efficient carbon fixation by cyanobacteria

CrossMark

(19). Carbon fixation in the Calvin cycle relies on the enzyme RuBisCO, which has a low turnover rate and, in addition to the fixation of carbon dioxide, also catalyzes the unproductive fixation of oxygen. RuBisCO is encapsulated within a protein shell together with carbonic anhydrase (CA). CA converts incoming bicarbonate (HCO_3^-) to CO_2, which accumulates within the compartment, thereby enhancing the carbon fixation reaction of RuBisCO and reducing the futile reaction with oxygen. Carboxysomes in different organisms are subdivided into α- and β-carboxysomes on the basis of the type of RuBisCO (IA versus IB) present in the particular species (20). The two classes of carboxysome also differ in their shell proteins, size, and internal organization and are thought to be the result of convergent evolution (19).

In recent years, much effort has been made to engineer carbon-concentrating mechanisms in plants, with the goal of enhancing photosynthetic efficiency and thus increasing crop yields (21–23). To this end, the introduction of carboxisomal RuBisCO into tobacco plants supported autotrophic growth (24). More broadly, there is increasing interest in using synthetic enzyme compartments for efficient synthesis of industrial chemicals and biofuels (25–27). However, despite the ubiquity of metabolic compartmentalization and its potential applications in synthetic biology, a quantitative understanding of the design principles and functional trade-offs of such compartments is still lacking.

Here, we use mathematical modeling to study how the size and enzymatic composition of compartments affect an encapsulated metabolic pathway. In particular, we ask how compartments should be constructed so as to maximize the enzymatic productivity. In the parameter regime of α-carboxysomes, we find that the optimal compartmentalization strategy is to form multiple compartments, each with at least a certain critical size, and each with less than maximal enzyme occupancy. Interestingly, the same productivity can be achieved for any compartment larger than a critical size, provided the enzyme densities are chosen appropriately. The enzyme arrangement within the compartment plays little role over the biologically relevant range of compartment sizes. We explain these phenomena with the aid of an analytically solvable model in which metabolites are well mixed within the compartment. We also characterize the qualitatively different compartmentalization strategies that emerge outside the well-mixed regime. Our results suggest that the different sizes and packing densities of α- and β-carboxysomes each represent an optimal strategy given the structures of their corresponding shell proteins.

MATERIALS AND METHODS

Model

We consider a subcellular compartment, shown schematically in Fig. 1 a, consisting of a selectively permeable shell that encapsulates enzymes of
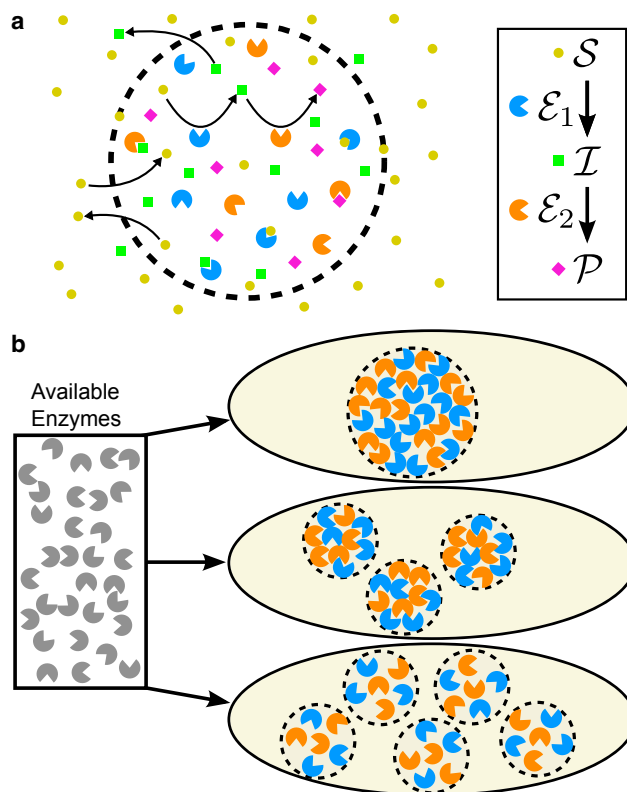

FIGURE 1 Illustration of the pathway model and compartmentalization strategies. (a) Model two-step enzymatic pathway with enzymes contained within a microcompartment. The permeable compartment shell allows for the exchange of metabolites $\mathcal{S}$ and $\mathcal{I}$ with the cytoplasm. (b) A fixed number of enzymes could be distributed according to many different compartmentalization strategies, each characterized by a particular compartment size, enzyme density, and ratio of $\mathcal{E}_1$ to $\mathcal{E}_2$ enzymes. Each such strategy would lead to a different pathway flux, and therefore a different productivity. To this figure in color, go online.

two types, $\mathcal{E}_1$ and $\mathcal{E}_2$. This shell may be composed of proteins, as in bacterial microcompartments, or a lipid bilayer, as is typical of eukaryotic organelles. Our model two-step pathway has the reaction scheme $\mathcal{S} \xrightarrow{\mathcal{E}_1} \mathcal{I} \xrightarrow{\mathcal{E}_2} \mathcal{P}$. Substrate molecules $\mathcal{S}$ enter the compartment from the cytoplasm through the boundary shell, and are converted by enzyme $\mathcal{E}_1$ into intermediate product $\mathcal{I}$, which is converted into final product $\mathcal{P}$ by enzyme $\mathcal{E}_2$. However, both $\mathcal{S}$ and $\mathcal{I}$ can also be lost from the compartment through the shell before reacting further. In principle, the intermediate product could also be unstable or consumed by side reactions within the compartment. In the Supporting Material, we discuss how this affects our results.

The total rate at which substrate $\mathcal{S}$ is converted into product $\mathcal{P}$ will depend on the number and size of compartments, the densities of the two enzymes, and the spatial arrangement of enzymes within the compartment. We refer to a particular choice for this collection of properties as a "compartmentalization strategy" (Fig. 1 b). Which compartmentalization strategy is the optimal one? Clearly, the answer to this question must depend on the objective or "design goal" of the system, as well as potential additional constraints. The biological imperative to achieve a high production flux while limiting the expenditure of resources in enzyme production (28) suggests that maximal enzymatic productivity is the design goal, with productivity defined as the total rate of $\mathcal{P}$ production per enzyme. In our theoretical study, we assume that the choice of compartmentalization strategy is otherwise not constrained in any significant way.

Productivity

Suppose that a cell contains a total of $N_\mathcal{E} = N_{\mathcal{E}_1} + N_{\mathcal{E}_2}$ copies of the enzymes $\mathcal{E}_1$ and $\mathcal{E}_2$, distributed equally over a number, N_c, of identical compartments, such that each compartment contains $E_c = N_\mathcal{E}/N_c$ enzymes. The total rate of production of $\mathcal{P}$ is given by $J_\mathcal{P} = N_c J_c$ where J_c is the rate of production per compartment. Then, the total production can be written as

$$J_\mathcal{P} = N_\mathcal{E} \frac{J_c}{E_c} \equiv N_\mathcal{E} \mathrm{P}, \tag{1}$$

where we define the productivity, P, as the flux of $\mathcal{P}$ production in one compartment divided by the total number of enzymes contained within the compartment. In steady-state, the productivity can also be written as $\mathrm{P} = J_{in}\ \epsilon/E_c$, where J_{in} is the total influx of substrate $\mathcal{S}$ across the compartment boundary and the factor $\mathcal{E}$, which we term the "conversion efficiency," is the probability that an $\mathcal{S}$ molecule entering the compartment will be converted into product $\mathcal{P}$, rather than leaving the compartment in the unreacted $\mathcal{S}$ or partially reacted $\mathcal{I}$ form.

The productivity allows us to quantify the performance of a given compartmentalization strategy, taking into account both the rate at which each compartment produces $\mathcal{P}$ and the necessary enzyme investment (how many such compartments can be constructed with the available enzymes). To isolate the effect of the compartmentalization strategy from processes happening at the scale of the cell as a whole, we will assume that the compartments do not affect one another via the cellular pools of metabolites $\mathcal{S}$ and $\mathcal{I}$, which we will take to be fixed. Under this assumption, the strategy that maximizes the productivity of a single compartment will also maximize the total production of $\mathcal{P}$ in the cell for a fixed number of enzymes, $N_\mathcal{E}$.

Reaction-diffusion model

To evaluate the productivity, we must specify the dynamics of $\mathcal{S}$ and $\mathcal{I}$ inside the compartment. We model the reactions of $\mathcal{S}$ with $\mathcal{E}_1$ and $\mathcal{I}$ with $\mathcal{E}_2$ using Michaelis-Menten kinetics, with $k_{cat}^{(1)}$ and $K_M^{(1)}$ the catalytic rate and the Michaelis constant of $\mathcal{E}_1$, and similarly for $\mathcal{E}_2$. We denote the density of enzymes of type $\mathcal{E}_1$ and $\mathcal{E}_2$ at position $\mathbf{r}$ within the compartment by $e_1(\mathbf{r})$ and $e_2(\mathbf{r})$, respectively. Enzymes are taken to be fixed in position, and thus, the density distributions do not vary over time. However, to account for the finite size of the enzymes, we impose as a constraint a maximal packing density of enzymes, $e_1(\mathbf{r}) + e_2(\mathbf{r}) \leq e_{max}$. Within the compartment, $\mathcal{S}$ and $\mathcal{I}$ are assumed to move by diffusion, with equal diffusion constants. The concentrations of $\mathcal{S}$ and $\mathcal{I}$, $s(\mathbf{r},t)$ and $i(\mathbf{r},t)$, respectively, therefore follow the coupled reaction-diffusion equations

$$\frac{\partial s(\mathbf{r},t)}{\partial t} = D\nabla^2 s(\mathbf{r},t) - \frac{k_{cat}^{(1)} e_1(\mathbf{r}) s(\mathbf{r},t)}{K_M^{(1)} + s(\mathbf{r},t)} \tag{2}$$

$$\frac{\partial i(\mathbf{r},t)}{\partial t} = D\nabla^2 i(\mathbf{r},t) + \frac{k_{cat}^{(1)} e_1(\mathbf{r}) s(\mathbf{r},t)}{K_M^{(1)} + s(\mathbf{r},t)} - \frac{k_{cat}^{(2)} e_2(\mathbf{r}) i(\mathbf{r},t)}{K_M^{(2)} + i(\mathbf{r},t)}. \tag{3}$$

The last term in Eq. 2 represents the conversion of $\mathcal{S}$ into $\mathcal{I}$ by $\mathcal{E}_1$, which appears as a local source of $\mathcal{I}$ in Eq. 3; the final term in Eq. 3 describes the conversion of $\mathcal{I}$ into $\mathcal{P}$ by $\mathcal{E}_2$. For simplicity, we consider compartments that are spherical, with radius R, and concentration profiles that are spherically symmetric.

We assume that through regulation of uptake and export rates, the cell maintains a homeostatic concentration, s_0, of substrate in the cytoplasm. Additionally, we assume that the intermediates are poorly retained by the cell membrane or rapidly degraded in the cytosol, such that their concentration in the cytoplasm is negligible. For carboxysomes in cyanobacteria, this assumption is reasonable, since detailed models of carboxysomes (29,30) predict that active conversion of CO_2 to HCO_3^- in the cytoplasm results

in a concentration of CO_2 outside the compartment ~1000-fold lower than inside. We describe exchange of metabolites across the compartment shell by the boundary conditions

$$D\frac{\partial s(r,t)}{\partial r}\bigg|_{r=R} = p_s[s_0 - s(R,t)] \tag{4}$$

$$D\frac{\partial i(r,t)}{\partial r}\bigg|_{r=R} = -p_i i(R,t), \tag{5}$$

where p_s and p_i are the permeabilities of the shell to $\mathcal{S}$ and $\mathcal{I}$.

In this model, a compartmentalization strategy consists of a particular choice for the radial enzyme concentration profiles, $e_1(r)$ and $e_2(r)$, and the compartment radius, R. For each such strategy, the steady-state productivity will be

$$\mathrm{P}\{e_1(r), e_2(r); R\} = \frac{\int_0^R 4\pi r^2 \frac{k_{cat}^{(2)} e_2(r) i(r)}{K_M^{(2)} + i(r)}\,\mathrm{d}r}{\int_0^R 4\pi r^2 [e_1(r) + e_2(r)]\mathrm{d}r}, \tag{6}$$

where $i(r)$ is the corresponding steady-state solution of Eqs. 2–5. In Eq. 6, the numerator is the total production flux of $\mathcal{P}$ per compartment, J_c, and the denominator is the total number of enzymes in one compartment, E_c (cf. Eq. 1). We will seek the compartmentalization strategy that optimizes P by maximizing Eq. 6 with respect to $e_1(r)$, $e_2(r)$, and R.

RESULTS

Our aim is to investigate generic features of optimal compartmentalization strategies that apply to microcompartments under both biological and synthetic conditions. We first study in detail the behavior of the model for parameters representative of one of the best-studied biological microcompartments, the α-carboxysome of cyanobacteria. We subsequently return to the question of how optimal compartmentalization strategies change in different parameter regimes. Additionally, we focus first on the linear regime of the Michaelis-Menten kinetics. As we will see later, including the full non-linear kinetics does not qualitatively alter the results of our analysis. We denote the catalytic efficiencies of the two enzymes in the linear regime by $\kappa_1 = k_{cat}^{(1)}/K_M^{(1)}$ and $\kappa_2 = k_{cat}^{(2)}/K_M^{(2)}$.

Optimal compartmentalization strategies for α-carboxysome parameters

The catalytic efficiencies of the two carboxysome enzymes, CA and RuBisCO, have been measured to be $\kappa_1 = 5\ (\mu M\ s)^{-1}$ and $\kappa_2 = 0.06\ (\mu M\ s)^{-1}$, respectively (31,32). Since we are unaware of direct measurements of permeability for the α-carboxysome shell, we estimated these parameters from the known structure of the shell proteins (33,34) ($p_s = 90\ \mu m\ s^{-1}$ and $p_i = 18\ \mu m\ s^{-1}$; see the Supporting Material for details). We used a metabolite diffusion coefficient $D = 1000\ \mu m^2 s^{-1}$ and a maximal enzyme concentration of $e_{max} = 25$ mM. For calculating

the productivity, we take a reference substrate concentration of $s_0 = 25$ μM.

We initially consider a scenario where both types of enzyme are uniformly distributed throughout the compartment, $e_1(r) = e_1$ and $e_2(r) = e_2$. Such a distribution may represent the case where the enzymes are freely diffusing. Under this assumption, the steady state of Eqs. 2–5 can be solved exactly to find an analytical expression for the productivity, $P(e_1, e_2; R)$ (see the Supporting Material). However, it is not possible to extract from this expression a closed form for the optimal values of e_1, e_2, and R. Instead, we optimized the productivity numerically. We visualized the results by plotting the optimal productivity, P^*, the optimal total enzyme concentration, $e_T^* = e_1^* + e_2^*$, and the optimal ratio of enzymes, $\phi^* = e_1^*/e_2^*$, for different values of R (see Fig. 2 a).

Examining first the optimal productivity (Fig. 2 a, top, green circles), we see that $P^*(R)$ increases with R up to a critical radius, R_c. Above R_c we see a broad plateau in the value of $P^*(R)$, indicating that similar productivity can be achieved over a wide range of compartment sizes that encompasses the entire biologically relevant range (from ~10 nm to ~3 μm, comparable to the size of cyanobacterial cells). For extremely large compartments, the productivity decreases gradually with increasing R.

The plateau in productivity is associated with a qualitative change in the optimal enzyme concentrations (Fig. 2 a, middle and bottom). For small compartments, $R < R_c$, maximizing productivity requires that compartments are maximally packed with enzymes, $e_T^* = e_1^* + e_2^* = e_{max}$. In contrast, for $R > R_c$, productivity is largest when $e_T^*(R) < e_{max}$; the optimal density shows a power-law dependence $e_T^*(R) \sim R^{-1}$. This tuning of the total enzyme density to the compartment size is crucial for generating the plateau in productivity observed in Fig. 2 a, top: if, instead, compartments are always maximally filled with enzymes, then the productivity shows a pronounced peak at $R = R_c$ and rapidly decreases for $R > R_c$ (Fig. 2 a, top, purple crosses). The optimal ratio of abundances of the two types of enzymes, $\phi^*(R) = e_1^*(R)/e_2^*(R)$, decreases with increasing R for $R < R_c$ before taking a constant value, ϕ_c^*, for $R > R_c$.

The optimal compartmentalization strategy for α-carboxysome parameters is therefore to produce enzymes of type $\mathcal{E}_1$ and $\mathcal{E}_2$ in the ratio ϕ_c^*, and to assign these to compartments of size $R > R_c$ such that the total enzyme density is $e_T^*(R) = e_{max}R_c/R$. For a compartment radius of $R = 60$ nm, the typical radius of an α-carboxysome (35), our analysis predicts that the optimal enzyme density is $\approx 30\%$ of the maximal packing density, e_{max}, resulting in a productivity that is ~ 30% higher than similarly sized compartments that are maximally packed (Fig. 2 a, top). Interestingly, α-cyanobacteria indeed contain several α-carboxysomes (36), each with just a quarter of the compartment volume occupied by RuBisCO enzymes (35). Thus, these cyanobacteria may have evolved to form a surplus of α-carboxysomes that are not fully packed to optimally exploit the cooperative activity of the encapsulated CA and RuBisCO.
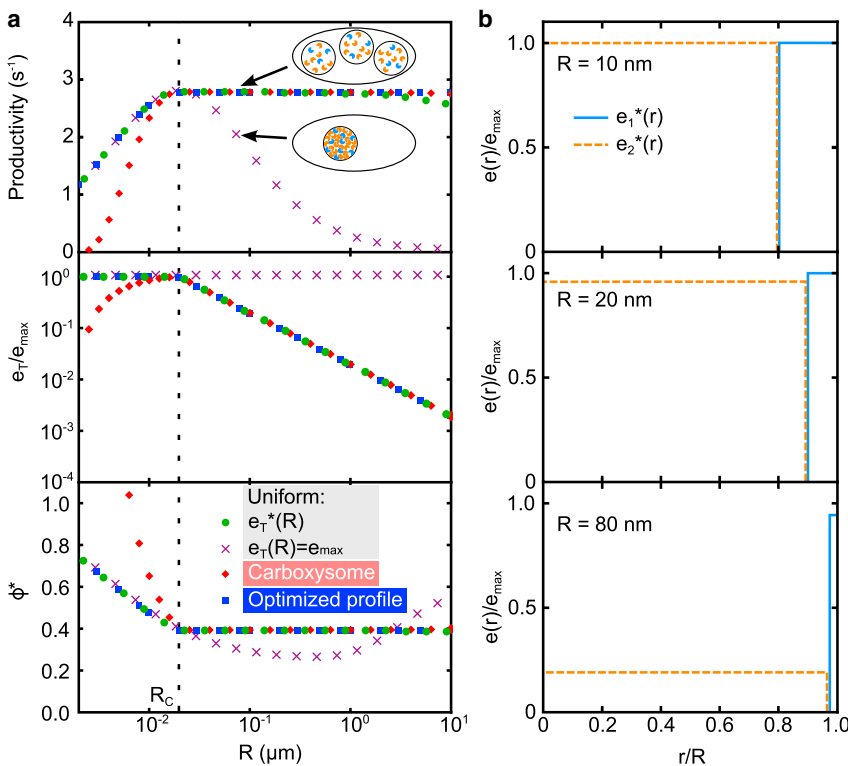

FIGURE 2 Optimal compartmentalization strategies for α-carboxysome parameters. (a) Optimal productivity (top), total enzyme density, $e_T^* = e_1^* + e_2^*$ (middle), and enzyme abundance ratio, $\phi^* = e_1^*/e_2^*$ (bottom) for four different arrangements of enzymes: uniform distribution at optimal density (green circles); uniform distribution at maximal density, $e_T = e_{max}$ (purple crosses); enzyme arrangement as observed in carboxysomes (Eq. 7; red diamonds); and optimized intracompartment enzyme arrangements (blue squares), as plotted in Fig. S1 in the Supporting Material. (b) Examples of the enzyme arrangements for the carboxysome configuration of Eq. 7 (with optimized e_1 and e_2 values) for different compartment sizes. To see this figure in color, go online.

So far we have assumed that the enzymes are uniformly distributed throughout the compartment. However, in naturally occurring microcompartments, the enzymes are in general not uniformly distributed. For example, in carboxysomes, CA is located at the inner surface of the protein shell, whereas RuBisCO is distributed throughout the compartment interior (37). Similarly, the locations of enzymes in synthetic microcompartments are often constrained by the method of enzyme encapsulation. For example, enzymes may be incorporated into the microcompartment by tethering them to shell proteins (38). This naturally raises the question of how the enzyme arrangement inside the compartment affects the productivity.

Focusing first on the enzyme arrangement observed in carboxysomes, we examined how the optimal compartmentalization strategy changes when $\mathcal{E}_1$ is restricted to a layer of thickness $\delta = 2$ nm (roughly the size of a small protein) at the compartment boundary while $\mathcal{E}_2$ is distributed throughout the remaining volume. We solved Eqs. 2–5 with

$$e_1(r) = \begin{cases} 0 & r \leq R - \delta \\ e_1 & r > R - \delta \end{cases}, e_2(r) = \begin{cases} e_2 & r \leq R - \delta \\ 0 & r > R - \delta \end{cases} \quad (7)$$

(see the Supporting Material) and again optimized the productivity with respect to e_1 and e_2, subject to the constraint $e_1, e_2 \leq e_{max}$ (Fig. 2 b).

For $R > R_c$, the optimal productivity and compartment-averaged enzyme densities, $(e_T^*(R) = V^{-1} \int_V [e_1(r) + e_2(r)] d^3 r, \phi^*(R) = \int_V e_1(r) d^3 r / \int_V e_2(r) d^3 r)$, are almost identical to those found for uniformly distributed enzymes (Fig. 2 a, red diamonds). Thus, the optimal compartmentalization strategy is not changed when the enzyme distribution is of the form in Eq. 7. For $R < R_c$, $e_T^*(R)$ and $\phi^*(R)$ differ from the optimal uniform enzyme distribution, and a lower productivity is achieved. However, this deviation arises simply because for fixed δ it is impossible to maximally pack the compartment while simultaneously maintaining a specific ratio of $\mathcal{E}_1$ to $\mathcal{E}_2$ enzymes.

Next, we determined numerically the full enzyme distributions $e_1^*(r)$ and $e_2^*(r)$ that maximize the productivity, subject only to the constraint $e_1(r) + e_2(r) \leq e_{max}$ (see the Supporting Material for details). The resulting optimal profiles change with the compartment radius, R, and differ substantially from a uniform enzyme distribution (see Fig. S1). Notably, though, the corresponding productivity is barely increased compared to that achieved by uniformly distributed enzymes (Fig. 2 a). Furthermore, the average densities of $\mathcal{E}_1$ and $\mathcal{E}_2$ over the entire compartment are the same as for uniform enzymes.

Together these results show that, for the chosen parameters, the precise arrangement of enzymes within the compartment does not significantly affect the productivity. What is most important is rather to ensure that the average density of enzymes within compartments is appropriately chosen according to their size.

Well-mixed approximation

Our observation that the intra-compartment enzyme arrangement has little impact on the productivity suggests that the spatial distribution of metabolites within the compartment is rather uniform. Indeed, we found that for $R \lesssim 1 \mu m$, where the productivities for different enzyme arrangements coincide, the densities $s(r)$ and $i(r)$ vary within the compartment by at most ~10% and ~1%, respectively. To understand for which parameter regimes such a uniform distribution of metabolites will apply, it is instructive to consider the various timescales that characterize the behavior of the system. Diffusive mixing of the metabolites throughout the compartment occurs on a timescale of $\tau_D \sim R^2 / D$. The reactions of metabolites with enzymes occur on the timescales $\tau_1 = 1/(\kappa_1 e_1)$ and $\tau_2 = 1/(\kappa_2 e_2)$. Finally, we identify two timescales associated with the exchange of metabolites across the compartment boundary, $\tau_s \sim R/p_s$ and $\tau_i \sim R/p_i$. The R-dependence of these latter timescales can be understood by considering the rate of exchange across the boundary to consist of the intrinsic (R-independent) crossing rate for a molecule that is located at the boundary multiplied by the fraction of the compartment volume that can be considered close to the boundary, which decreases as R^{-1}.

Metabolites within the compartment can be considered well mixed when the diffusive timescale is short compared to those of reaction and exchange, $\tau_D \ll \tau_{1,2}, \tau_{s,i}$. In this limit, metabolites effectively sample the entire pool of enzymes before they leak through the boundary or react. It is then plausible that the pathway flux does not depend on the precise arrangement of enzymes within the compartment. From the R-dependence of the different timescales, we can see that τ_D will be smaller than the other timescales when R is sufficiently small. For the parameters and optimal enzyme concentrations of Fig. 2, we estimated that this will be the case for $R \lesssim 1.4 \mu m$, which is much larger than the typical size of BMCs and the critical radius, R_c. Hence, assuming that the contents of BMCs are well mixed appears to be a good approximation for biologically relevant compartment sizes.

To gain further insight into the optimal compartmentalization strategy, we therefore analyzed a simplified version of our model where the reactants $\mathcal{S}$ and $\mathcal{I}$ are well mixed within the compartment. Assuming that the reactants flowing across the boundary are rapidly distributed throughout the compartment, the steady-state equations for s and i become

$$0 = 4\pi R^2 p_s (s_0 - s) - \frac{4}{3}\pi R^3 \kappa_1 e_1 s \quad (8)$$

$$0 = 4\pi R^2 p_i (-i) + \frac{4}{3}\pi R^3 (\kappa_1 e_1 s - \kappa_2 e_2 i), \quad (9)$$

where the first term in each equation describes the net transport flux across the compartment boundary and the second term corresponds to the reaction flux. To compare with the

results of Fig. 2, we solve Eqs. 8 and 9 for the productivity as a function of the total enzyme concentration, $e_T = e_1 + e_2$, and the ratio of enzyme densities, $\phi = e_1/e_2$,

$$P(e_T, \phi, R) = \frac{3 p_s s_0}{e_T R}$$

$$\times \underbrace{\left[\frac{\phi e_T R}{\frac{3 p_s}{\kappa_1}(1 + \phi) + \phi e_T R} \right] \left[\frac{e_T R}{\frac{3 p_i}{\kappa_2}(1 + \phi) + e_T R} \right]}_{\epsilon(e_T, \phi, R)}. \quad (10)$$

The total enzyme density, e_T, and radius, R, appear in the productivity only as the product $e_T R$, which immediately implies a scaling $e_T^*(R) \sim R^{-1}$. From Eqs. 8–10, we see that this R-dependence originates in the need to balance metabolite transport across the compartment boundary, which depends on the surface area, $j_{s,i} \propto p_{s,i} A \sim R^2$, against the flux of enzymatic reactions, which occur throughout the compartment volume, $j_{1,2} \propto \kappa_{1,2} e_{1,2} V \sim e_{1,2} R3$. By choosing $e_{1,2} \sim A/V \sim R^{-1}$, the ratio of transport to reaction fluxes can be held fixed at the particular level that achieves maximal productivity. However, since the enzyme density e_T cannot exceed e_{max}, this scaling cannot be satisfied for all R. Optimizing the productivity with the constraint $e_T(R) \leq e_{max}$, we obtain

$$e_{T,wm}^*(R) = e_{max} \begin{cases} 1 & R \leq R_{c,wm} \\ R_{c,wm}/R & R > R_{c,wm} \end{cases},$$

$$\phi_{wm}^*(R) = \begin{cases} \left[\dfrac{1 + R/\lambda_2}{1 + R/\lambda_1} \right]^{1/2} & R \leq R_{c,wm} \\[3mm] \left[\dfrac{\lambda_1}{\lambda_2} \right]^{1/3} & R > R_{c,wm} \end{cases}, \quad (11)$$

where the critical radius $R_{c,wm} = \lambda_1^{2/3}\lambda_2^{1/3} + \lambda_2^{2/3}\lambda_1^{1/3}$ and the length scale parameters $\lambda_1 = 3 p_s/(\kappa_1 e_{max})$ and $\lambda_2 = 3 p_i/(\kappa_2 e_{max})$ correspond to the compartment radii at which the maximal turnover of substrate/intermediate via enzymatic reaction equals the rate of loss across the compartment boundary. The optimal productivity is then

FIGURE 3 Results of well-mixed approximation. Shown are the optimal productivity (*top*), the enzyme density, e_T^* (*middle*), and the ratio of $\mathcal{E}_1$ to $\mathcal{E}_2$ enzymes, ϕ^* (*bottom*). Data points show numerical optimization of the analytical expression for productivity for uniform enzymes, as in Fig. 2 *a*. Blue and orange dashed lines are the corresponding optima in the well-mixed approximation (Eqs. 11 and 12). The dashed green line shows the leading-order correction to the optimal productivity (Eq. 13). To see this figure in color, go online.

Thus, the well-mixed model correctly describes the optimal compartmentalization strategy for α-carboxysome parameters.

We can now also understand the trends in $e_T^*(R)$ and $\phi^*(R)$ observed in Fig. 3 across the full range of compartment sizes. The densities of substrate and intermediate in-

$$P_{wm}^*(R) = \begin{cases} \dfrac{\gamma \lambda_1 \lambda_2}{R(R + \lambda_1 + \lambda_2)^2} \left[\left\{ 1 + \dfrac{R(R + \lambda_1 + \lambda_2)}{\lambda_1 \lambda_2} \right\}^{1/2} - 1 \right]^2 & R \leq R_{c,wm} \\[5mm] \dfrac{\gamma}{\left[\lambda_1^{1/3} + \lambda_2^{1/3} \right]^3} & R > R_{c,wm} \end{cases}, \quad (12)$$

with $\gamma = 3 p_s s_0/e_{max}$. Equations 11 and 12 are in excellent agreement with the numerical optimization of the full reaction-diffusion model (Fig. 3), except at the largest R values.
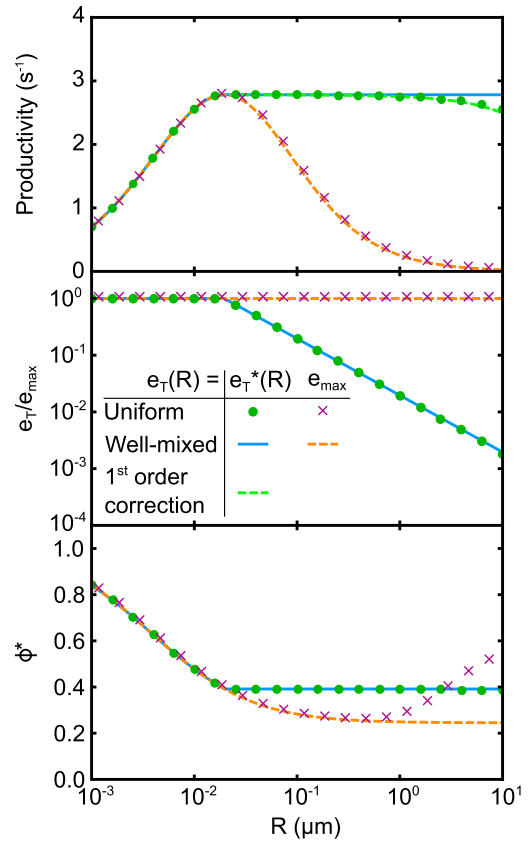
side the compartment are determined by two effects: exchange across the boundary, and production and consumption in enzymatic reactions. In particular, reactions

deplete the available pool of metabolites, reducing the efficiency with which enzymes can operate. In small compartments, $R < R_c$, exchange dominates over the effects of enzymatic reactions. Then the most productive strategy is to pack as many enzymes as possible into the compartment; the ratio of $\mathcal{E}_1$ to $\mathcal{E}_2$ enzymes should be chosen so as to balance the relative depletion of $\mathcal{S}$ and $\mathcal{I}$, thereby maximizing the efficiency with which $\mathcal{S}$ is converted into $\mathcal{P}$. As R increases toward R_c, the larger number of enzymes in the compartment increases the impact of enzymatic reactions on the metabolite concentrations, which in turn leads to diminishing returns in conversion efficiency (reflected in the saturation of $\mathcal{E}$ at large R). At the same time, the investment of enzymes needed to maintain fully packed compartments, represented by the prefactor $(e_{\mathrm{T}}R)^{-1}$ in the productivity, continues to increase with R. The critical radius $R_{\mathrm{c,wm}}$ represents the compartment size at which the rate of increase of the product flux exactly matches the increasing cost of maintaining fully packed compartments. For $R > R_{\mathrm{c,wm}}$, the productivity of maximally packed compartments becomes smaller than could be achieved by constructing a larger number of partially filled compartments.

Note that the $\sim R^{-1}$ scaling of the optimal enzyme concentrations and the plateau in optimal productivity rely not only on the fast diffusive mixing but also on the loss of intermediate exclusively through the compartment boundary. If intermediates were also to decay within the compartment volume, the optimal compartmentalization strategy, including the optimal enzyme densities, would change (see the Supporting Material for further details).

Breakdown of the well-mixed approximation

For large compartment radii we see that the numerically-optimized productivity deviates from the prediction of the well-mixed model (Fig. 3 top, $R \gtrsim 10 \ \mu$m). This is to be expected because the mixing timescale $\tau_D \sim R^2$ increases more rapidly for large R than the other timescales in the system, which scale at most linearly with R. To examine systematically the deviation from the fast-diffusion regime, we performed a series expansion of P^* in powers of D^{-1}, obtaining

$$\mathrm{P}^*(R) = \mathrm{P}^*_{\mathrm{wm}}\left[1 + \frac{(p_i - p_s)R}{5(1 + \phi^*_{\mathrm{wm}})D} + O(D^{-2})\right]. \quad (13)$$

(See the Supporting Material for further details and the case $p_i \approx p_s$.) The first-order correction to the productivity (see Fig. 3 top, green dashed line) is due to the appearance of spatial gradients of $\mathcal{S}$ and $\mathcal{I}$. Changes in the optimal enzyme concentrations away from their well-mixed values enter only in higher-order terms.

From Eq. 13, we can identify the compartment size, $R_x \sim 5D(1 + \phi^*_{\mathrm{wm}})/|p_i - p_s|$ (for the case $p_s = p_i = p$, $R_x \sim \sqrt{175/3}(D/p)$; see the Supporting Material), at

which the optimal productivity is expected to deviate significantly from the well-mixed result. Interestingly, P^* can either increase or decrease relative to its well-mixed value depending on which of p_s or p_i is larger. This is because the explicit diffusion of metabolites has opposing effects on the efficiencies of the two reaction steps. The rate of $\mathcal{S}$ - $\mathcal{E}_1$ reactions is reduced in the center of the compartment, because fewer of the $\mathcal{S}$ molecules that are introduced at the boundary diffuse into the center. Conversely, those $\mathcal{I}$ molecules that are produced away from the compartment boundary have a significantly increased probability of reacting with $\mathcal{E}_2$ rather than escaping compared to the well-mixed scenario, leading to a higher probability of conversion of $\mathcal{I}$ to $\mathcal{P}$. The relative values of D/p_s and D/p_i, which represent the length scales over which $\mathcal{S}$ and $\mathcal{I}$ molecules can be considered "close" to the boundary, determine which of these effects has a larger impact on the pathway flux. In most biological contexts, we would expect compartments to primarily confine intermediates, rather than limiting the influx of substrates, suggesting that $p_s > p_i$ is the more natural condition. In this case, as in Fig. 3, the productivity decreases at large R.

If alternative biochemical processes that give rise to concentration gradients, such as the spontaneous decay of intermediates, were also to take place in the system, this may cause both greater deviation from the well-mixed approximation and also breakdown of the approximation at smaller values of R (see the Supporting Material).

Compartmentalization strategies for highly permeable shells

If the shell permeability is sufficiently high, the well-mixed approximation can break down at compartment sizes comparable to or even smaller than the compartment size at which the transition to sub-maximal packing would occur, $R_x \lesssim R_{\mathrm{c,wm}}$. In such cases, we should not necessarily expect a plateau in productivity as predicted by the well-mixed model. We therefore investigated how the optimal compartmentalization strategies change when one or both of the shell permeabilities is set to a value of $p = 10^4 \ \mu$m s^{-1}, such that R_x lies in the range of physically realistic compartment sizes ($R = 0.01$–$1 \ \mu$m).

We again consider first the case of uniformly distributed enzymes. For this enzyme arrangement, we observe that some common features are shared between the optimal compartmentalization strategies in the different parameter regimes (Fig. 4, a–c, green circles). In all cases, we can again identify a critical radius, R_c, at which a distinct transition in the optimal enzyme density occurs. For $R < R_c$, the optimal compartment is maximally packed; for $R > R_c$, the optimal enzyme density, $e^*_{\mathrm{T}} < e_{\mathrm{max}}$, and the productivity again exceed those of maximally packed compartments of similar size (Fig. 4, purple crosses). However, the critical radii differ from those predicted by the well-mixed model (Fig. 4, a–c, blue lines), $R_{\mathrm{c,wm}}$.
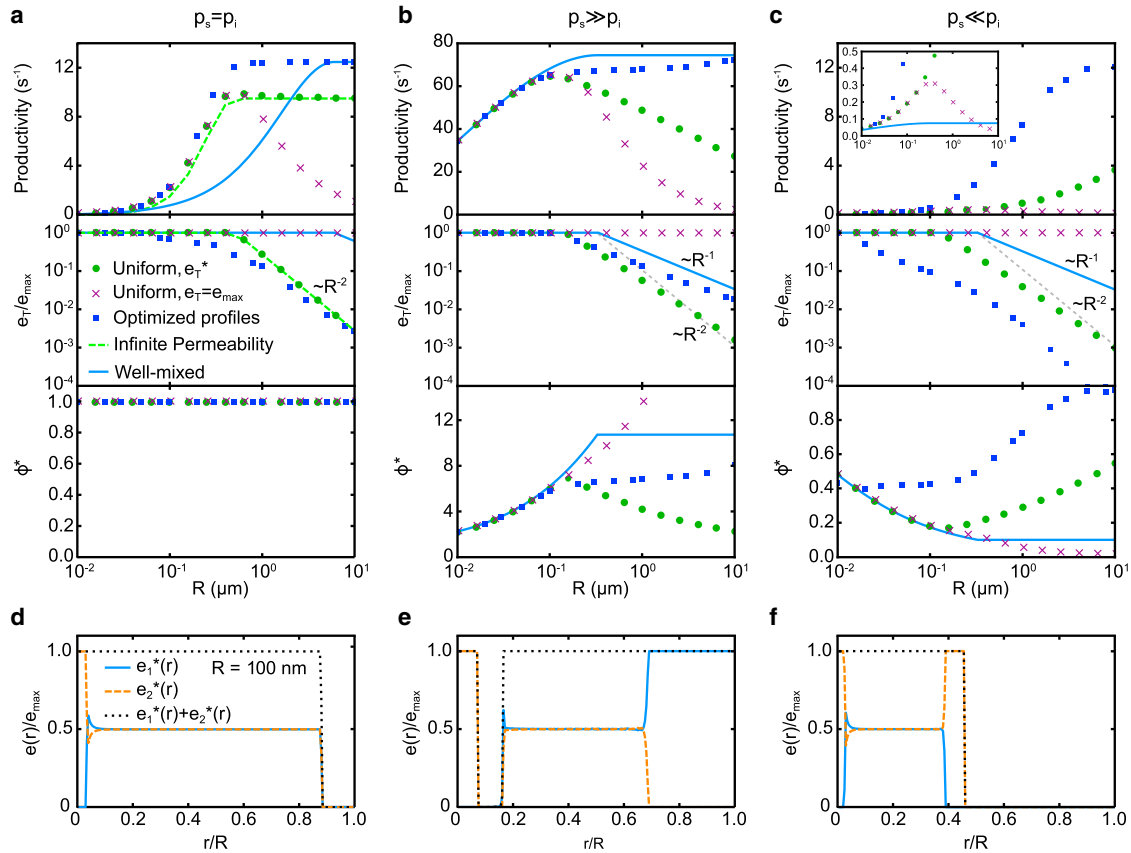
FIGURE 4 Optimal compartmentalization strategies outside the well-mixed regime. (*a–c*) Optimal productivity and corresponding enzyme densities as a function of the compartment radius for boundary permeabilities $p_s = p_i = 10^4 \ \mu m \ s^{-1}$ (*a*); $p_s = 10^4 \ \mu m \ s^{-1}$, $p_i = 10 \ \mu m \ s^{-1}$ (*b*); and $p_s = 10 \ \mu m \ s^{-1}$, $p_i = 10^4 \ \mu m \ s^{-1}$ (*c*). Other parameters are fixed at $\kappa_1 = \kappa_2 = 0.4 \ (\mu M \ s)^{-1}$, $e_{max} = 25 \ mM$, $s_0 = 250 \ \mu M$, and $D = 100 \ \mu m^2 \ s^{-1}$. The limit $p_s, p_i \to \infty$ (see the Supporting Material) is shown as a green dashed line. (*d–f*) Optimal concentration profiles for the three cases above at a compartment radius of $R = 100 \ nm$. To see this figure in color, go online.

Beyond these similarities, we also observe qualitative differences between the optimal compartmentalization strategies. When both p_s and p_i are large (Fig. 4 *a*), we find a plateau in the productivity above R_c. We observe that the optimal enzyme density in compartments decreases as $e_T^* \sim R^{-2}$, in contrast to the low-permeability regime, where we found $e_T^* \sim R^{-1}$. Furthermore, examining the solution for the productivity in the limit $p_{s,i} \to \infty$, we find that e_T and R appear only as the product $e_T R^2$ (see the Supporting Material). This result allows us to identify the origin of the different scaling in the different processes governing exchange of reactants with the environment. In the low-p limit, the overall exchange rate is determined by the fraction of the compartment volume that is proximal to the boundary, which decreases as $\sim R^{-1}$. On the other hand, in the high-p regime, exchange is limited by the time taken to diffuse to the boundary, which scales as $\tau_D \sim R^2$. Yet, despite the different underlying dynamics, the optimal compartmentalization strategy resembles that in the low-permeability regime, consisting of compartments larger than R_c with the appropriately chosen $e_T^*(R)$ and ϕ^*.

In contrast, when only one of p_s and p_i is large, the optimal productivity does not exhibit a plateau for $R > R_c$. Rather, when p_s is small and p_i is large (Fig. 4 *c*), the optimal productivity steadily increases with the compartment size. Thus, large, sparsely occupied compartments are the most productive. Since in this parameter regime productivity is limited by the rapid escape of $\mathcal{I}$ across the boundary, compartments should contain more $\mathcal{E}_2$ than $\mathcal{E}_1$ ($\phi^* < 1$). Conversely, when p_s is large and p_i is small (Fig. 4 *b*), the productivity exhibits a pronounced maximum at a certain radius, $R^* \approx R_c$. The optimal compartmentalization strategy here is to produce compartments of size $R = R^*$ that are maximally packed, $e_T^*(R^*) = e_{max}$. More enzymes of type $\mathcal{E}_1$ than of type $\mathcal{E}_2$ are required ($\phi^* > 1$) to exploit the $\mathcal{S}$ that diffuses rapidly across the compartment boundary, whereas the slow leakage of $\mathcal{I}$ means that this metabolite will accumulate inside the compartment.

In the well-mixed regime, changing the intra-compartment arrangement of enzymes has little effect on the productivity (Fig. 2 *a*), since metabolites explore the entire compartment before reacting. However, if the compartment is not well mixed, we expect that the specific choice of

enzyme arrangement will significantly affect the reaction flux. We therefore investigated numerically the enzyme profiles $e_1(r)$ and $e_2(r)$ that maximized productivity. Examples of the resulting optimal enzyme profiles are shown in Fig. 4, d–f. The corresponding metabolite density profiles are shown in Fig. S2 in the Supporting Material.

Fig. 4, a–c (blue squares), confirms that by a suitable choice of $e_1(r)$ and $e_2(r)$ it is possible to achieve a higher productivity than with uniformly distributed enzymes. The advantage is more significant when only one of p_s and p_i is large, rather than when both permeabilities are high. We can understand how the increased productivity comes about by examining the main features of the optimal enzyme profiles (the fine-scale details of the enzyme distributions, in particular at small r values, are susceptible to discretization artifacts and do not significantly affect the value of P). When p_s is large and p_i is small (Fig. 4 e), enzymes of type $\mathcal{E}_1$ form a shell at the outer boundary of the compartment to maximize reactions with substrate $\mathcal{S}$ as it enters the compartment. Since the leakage of intermediate is slow, $\mathcal{E}_2$ enzymes can be localized to the interior side of this $\mathcal{E}_1$ band without seriously compromising the pathway flux. This enzyme arrangement requires more enzymes per compartment (larger e_T^* (Fig. 4 b, middle)) than the best uniform-enzyme strategy, meaning that fewer compartments with more enzymes yield a larger product formation rate. When p_s is small and p_i is large, enzymes of both types are concentrated in the center of the compartment (Fig. 4 f). Localizing $\mathcal{E}_1$ enzymes in this way ensures that $\mathcal{I}$ is produced far from the compartment boundary. $\mathcal{E}_2$ enzymes colocalize with $\mathcal{E}_1$ and also form a shell at the outer edge of the $\mathcal{E}_1$ domain to maximize the probability of capturing $\mathcal{I}$ molecules before they diffuse out of the compartment. By arranging enzymes in this way, each compartment can achieve a similar reaction with significantly fewer enzymes per compartment (smaller e_T^* (Fig. 4 c, middle)), such that a larger number of similar compartments can be constructed with the pool of available enzymes. Thus, the optimal compartmentalization strategies deviate qualitatively from those in the uniform-enzyme scenario.

Michaelis-Menten kinetics

So far, we have considered only the regime of low metabolite concentrations where the Michaelis-Menten reaction kinetics become linear in substrate concentration. However, this may not be the case in general. We therefore sought to understand how the full reaction kinetics alter the optimal compartmentalization strategies. We previously saw that the breakdown of the well-mixed approximation is due to the appearance of metabolite gradients. We therefore hypothesized that the inclusion of non-linear reaction kinetics would mitigate this breakdown through two effects. First, relative to linear kinetics with the same value of $\kappa = k_{cat}/K_M$, the effective reaction rate will be reduced by a factor of

$(1 + s/K_M^{(1)})^{-1}$ or $(1 + i/K_M^{(2)})^{-1}$. This suppresses the consumption of metabolites in metabolic reactions and, therefore, the appearance of metabolite concentration gradients. Second, even if gradients of metabolites form, they would only lead to differences in reaction rate at different positions if the absolute concentration were also to drop below the K_M value of the enzyme. For reactions that are in the zero-order regime, there will be no difference in reaction flux regardless of where in the compartment the enzymes are placed.

To test this hypothesis we calculated expressions for the densities of $\mathcal{S}$ and $\mathcal{I}$ and productivity, $P(e_1, e_2, R)$, in a well-mixed model taking into account the Michaelis-Menten kinetics (see the Supporting Material), which we again optimized numerically with respect to $e_T(R)$ and $\phi(R)$. Additionally, we determined the optimal $e_T(R)$ and $\phi(R)$ for the full non-linear reaction-diffusion system, Eqs. 2 and 3, with uniform enzymes; since an analytic solution of the non-linear boundary-value problem is not possible, the steady-state metabolite concentrations were also calculated numerically in this case (see the Supporting Material). The extent of enzyme saturation was varied by changing the external substrate concentration, s_0.

The qualitative characteristics of the optimal compartments are similar to the linear reaction regime (see Fig. 5). In particular, we again observe a plateau in $P^*(R)$ above a critical radius, R_e, accompanied by a decrease in

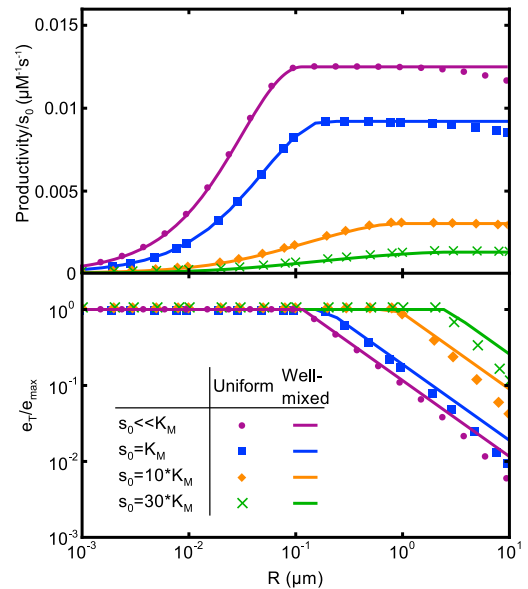FIGURE 5 Optimal compartmentalization strategies with Michaelis-Menten reaction kinetics. Optimal productivity (top) and total enzyme concentration (bottom) for different external substrate concentrations, s_0, are shown. Data points show results of numerical optimization for the reaction-diffusion model (Eqs. 2 and 3) with a uniform distribution of enzymes. Solid lines show the corresponding optimization in the well-mixed approximation. Reaction parameters were chosen to resemble the activity of an "average" enzyme, $k_{cat}^{(1)} = k_{cat}^{(2)} = 10$ s^{-1} and $K_M^{(1)} = K_M^{(2)} = 100$ μM (55). Other parameters were $D = 100$ μm^2 s^{-1} and $p_s = p_i = 50$ μm s^{-1}. To see this figure in color, go online.

the total enzyme density, $e_{\mathrm{T}}^*(R) \sim R^{-1}$. However, as the extent of saturation is increased, the maximal productivity increases sub-linearly with s_0, and R_c also increases. As in the case of linear reactions, the transition to sub-maximally packed compartments occurs when depletion of metabolites by reactions, which increases with the number of enzymes in a compartment, reaches such an extent that the gain in product formation from maintaining fully packed compartments is less than the corresponding cost in terms of available enzymes. When the encapsulated enzymes are saturated, however, depletion of metabolites will have a negligible effect on the reaction flux. For there to be a significant impetus to reduce the enzyme density inside the compartment, the number of enzymes must become so large as to deplete the metabolite pool into the range where enzymes are no longer saturated. Thus, the transition to sub-maximally packed compartments occurs at larger compartment sizes as the supply of $\mathcal{S}$ is increased.

As expected, we find excellent agreement between the well-mixed approximation and the reaction-diffusion model under biologically realistic low-permeability conditions. We therefore conclude that the well-mixed approximation also provides an excellent model for compartmentalization in the non-linear regime. At large $R > 1~\mu m$, we observe some deviation in the productivity for unsaturated conditions, $s_0 \lesssim K_{\mathrm{M}}$, in the same way as for the linear regime. However, for $s_0 \gg K_{\mathrm{M}}$, the same radius falls in the range $R < R_c$, and the optimal compartmentalization strategy still appears to track the well-mixed result. In particular, a difference in the optimal enzyme densities is only observed for $R > R_c$, corresponding to the point at which the enzymes within the compartment first become less than fully saturated.

DISCUSSION

We have investigated the design principles underlying enzyme compartmentalization for a simple model metabolic pathway. We found that the strategy of packing enzymes into compartments as densely as possible only provides the highest productivity if compartments are constrained to be very small. On the other hand, if compartments can exceed a critical size, the productivity is optimized by constructing large compartments, each of which is less than maximally packed with enzymes. In the parameter regime of low membrane permeabilities that includes α-carboxysomes, it is reasonable to assume that metabolites are well mixed throughout the compartment. Therefore, the precise arrangement of enzymes within the compartments is of little importance in determining the productivity. Furthermore, similar productivity can be achieved across a wide range of compartment sizes, provided that the enzyme concentration is appropriately chosen according to the compartment radius. These results provide a guide for the construction of efficient synthetic bioreactors.

We have focused on parameters that resemble α-carboxysome microcompartments, one of the best-studied metabolic microcompartments. Interestingly, β-carboxysome shells were found to have larger pores than those of α-carboxysomes (18,33). We estimate that the shell permeability of β-carboxysomes is ~12-fold higher than that of α-carboxysomes. This leads to a larger critical radius, R_c, at which the optimal strategy switches from maximal to partial packing of enzymes, but it also means that the well-mixed regime for β-carboxysomes is limited to smaller compartments (corresponding to a smaller R_x), resulting in a more pronounced maximum in the optimized productivity (Fig. 6). Notably, the typical size of β-carboxysomes, which is larger than that of α-carboxysomes (150 nm vs. 60 nm (39)), lies close to the radius at which our model predicts maximal productivity. The optimal strategy at this compartment size is maximal packing of enzymes. In contrast, α-carboxysomes fall in the regime $R > R_c$ for which we predict the optimal strategy to be partial packing. Interestingly, the arrangement of RuBisCO within β-carboxysomes was described as densely packed or paracrystalline (40), in contrast to the less organized packing observed within α-carboxysomes (35,41). Our analysis suggests that the observed differences in carboxysome properties may reflect the different optimal compartmentalization solutions that arise given the specific properties of each protein shell.
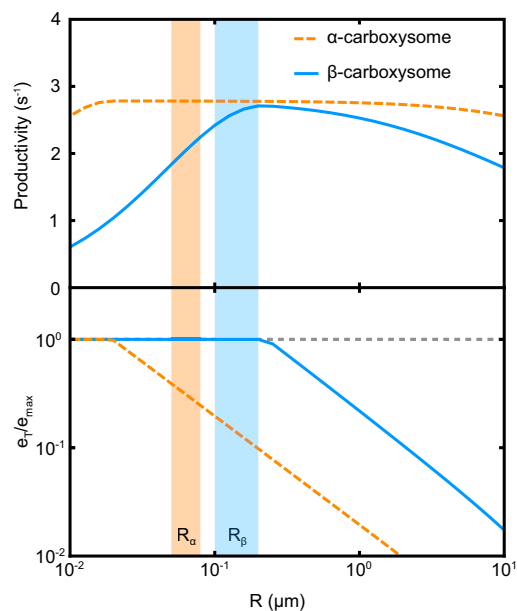

FIGURE 6 Comparison of optimal compartmentalization strategies for α- and β-carboxysomes. The higher shell permeability of β-carboxysomes (*blue line*) ($p_s = 1080~\mu m~s^{-1}$, $p_i = 215~\mu m~s^{-1}$) shifts the optimal productivity curve toward larger compartment radii and leads to a more pronounced productivity maximum compared to α-carboxysomes (*orange dashed line*) ($p_s = 90~\mu m~s^{-1}$, $p_i = 18~\mu m~s^{-1}$). Typical size ranges for the two carboxysome types are denoted by the shaded regions. To see this figure in color, go online.

Our aim in this work has been to explore some of the generic properties of compartmentalization strategies. Our simplified reaction-diffusion model omits a number of biochemical details of metabolic reactions. For example, product inhibition will tend to reduce the efficiency of enzymes as the concentration of $\mathcal{P}$ becomes larger, thereby providing a further incentive to reduce the enzyme concentration within a compartment to reduce the rate of $\mathcal{P}$ production and hence also its concentration. This potentially leads to a shift of the critical radius to smaller radii and a change in the scaling of e_T, but the qualitative transition from maximally packed to sparsely packed compartments will persist. We have furthermore neglected the discrete nature and spatial structure of enzyme molecules. Macromolecular crowding can have many effects, such as reducing metabolite diffusivity (42) and enhancing reaction kinetics (43,44). We do not believe such effects will be significant in most biological microcompartments, since the metabolites involved are typically small molecules such as CO_2 or H_2O_2, whose diffusion will be little affected by obstructions on the much larger scale of enzyme molecules. However, if metabolites were themselves large, then crowding may potentially increase the benefit of specific enzyme arrangements that promote trapping or channeling of reactants. The discreteness of enzymes means that there will inevitably be fluctuations in the number of enzymes between compartments. It has previously been shown that such variability can alter the optimal strategy for partitioning signaling proteins among different sub-domains (45). It remains to be seen whether a similar effect occurs in the context of metabolic reactions.

It is also possible for the reactions within compartments to become coupled through exchange of intermediates or depletion of substrate in the cytoplasm. It will be interesting to see under which conditions such inter-compartment interactions, which will be governed by the same physical processes of diffusion and exchange across compartment and cell boundaries as our intra-compartment model, alter the optimal compartmentalization strategies for the cell as a whole.

Although we have considered only the steady-state productivity of static compartment configurations, metabolism is a highly dynamic and tightly regulated collection of processes. In scenarios where maximizing productivity is not the principal design goal, our model nevertheless demonstrates that metabolic fluxes may be controlled by changing the number and size of organelles in which reactions take place. Multiple examples are known of systems in which such changes in sub-cellular organelles are induced in response to varying metabolic demands or environmental cues (46–48). That changing compartmentalization can alter metabolic flux has been demonstrated in the fungus *Penicillium chrysogenum*. Overproduction of a peroxisomal membrane protein resulted in a significant increase in the number of peroxisomes (49), which in turn led to a 2.5-fold increase in the level of penicillin in the culture medium. Interestingly, the amounts of peroxisomal enzymes involved in penicillin biosynthesis were unchanged compared to the control strain; rather, enzymes were distributed over a larger number of smaller organelles. It would be of interest to observe penicillin production if the peroxisomes are further divided into even smaller organelles. Our analysis predicts that at a certain organelle size, the production of penicillin would decrease again due to the increasing loss of intermediates.

In addition to changing compartment size and number, cells are also able to regulate the morphology of organelles. For example, studies have shown that mitochondria change their shape according to the energy demands of the cell (50,51). This morphological change was suggested to be an active mechanism to increase bio-energetic efficiency (51). Proteinaceous microcompartments could also potentially be constructed with different morphologies depending on the abundance of different shell proteins (52). Our model predicts that for rapidly diffusing metabolites, productivity depends crucially on the surface area/volume ratio of compartments, whereas the specific geometry will be less important. Thus, adapting an organelle's surface/volume ratio by altering its shape presents an alternative possibility for tuning metabolic fluxes without altering enzyme expression levels.

SUPPORTING MATERIAL

Supporting Materials and Methods and three figures are available at http://www.biophysj.org/biophysj/supplemental/S0006-3495(16)34263-1.

AUTHOR CONTRIBUTIONS

All authors designed research. F.H. and F.T. performed research and analyzed data. All authors wrote the paper.

ACKNOWLEDGMENTS

SUPPORTING CITATIONS

References (53,54) appear in the Supporting Material.

REFERENCES

1. Reed, L. J. 1974. Multienzyme complexes. *Acc. Chem. Res.* 7:40–46.

2. Srere, P. A. 1987. Complexes of sequential metabolic enzymes. *Annu. Rev. Biochem.* 56:89–124.

3. An, S., R. Kumar, …, S. J. Benkovic. 2008. Reversible compartmentalization of de novo purine biosynthetic complexes in living cells. *Science.* 320:103–106.

4. Campanella, M. E., H. Chu, and P. S. Low. 2005. Assembly and regulation of a glycolytic enzyme complex on the human erythrocyte membrane. *Proc. Natl. Acad. Sci. USA.* 102:2402–2407.

5. Sampson, E. M., and T. A. Bobik. 2008. Microcompartments for B$_{12}$-dependent 1,2-propanediol degradation provide protection from DNA and cellular damage by a reactive metabolic intermediate. *J. Bacteriol.* 190:2966–2971.

6. Agapakis, C. M., P. M. Boyle, and P. A. Silver. 2012. Natural strategies for the spatial optimization of metabolism in synthetic biology. *Nat. Chem. Biol.* 8:527–535.

7. Hult, K., and P. Berglund. 2007. Enzyme promiscuity: mechanism and applications. *Trends Biotechnol.* 25:231–238.

8. Lee, H., W. C. DeLoache, and J. E. Dueber. 2012. Spatial organization of enzymes for metabolic engineering. *Metab. Eng.* 14:242–251.

9. Spivey, H. O., and J. Ovádi. 1999. Substrate channeling. *Methods.* 19:306–321.

10. Wheeldon, I., S. D. Minteer, …, M. Sigman. 2016. Substrate channelling as an approach to cascade reactions. *Nat. Chem.* 8:299–309.

11. Buchner, A., F. Tostevin, and U. Gerland. 2013. Clustering and optimal arrangement of enzymes in reaction-diffusion systems. *Phys. Rev. Lett.* 110:208104.

12. Buchner, A., F. Tostevin, …, U. Gerland. 2013. Optimization of collective enzyme activity via spatial localization. *J. Chem. Phys.* 139:135101.

13. Castellana, M., M. Z. Wilson, …, N. S. Wingreen. 2014. Enzyme clustering accelerates processing of intermediates through metabolic channeling. *Nat. Biotechnol.* 32:1011–1018.

14. Zecchin, A., P. C. Stapor, …, P. Carmeliet. 2015. Metabolic pathway compartmentalization: an underappreciated opportunity? *Curr. Opin. Biotechnol.* 34:73–81.

15. del Río, L. A., L. M. Sandalio, …, F. J. Corpas. 1992. Metabolism of oxygen radicals in peroxisomes and cellular implications. *Free Radic. Biol. Med.* 13:557–580.

16. Gantt, E., and S. F. Conti. 1969. Ultrastructure of blue-green algae. *J. Bacteriol.* 97:1486–1493.

17. Shively, J. M., G. L. Decker, and J. W. Greenawalt. 1970. Comparative ultrastructure of the thiobacilli. *J. Bacteriol.* 101:618–627.

18. Kerfeld, C. A., M. R. Sawaya, …, T. O. Yeates. 2005. Protein structures forming the shell of primitive bacterial organelles. *Science.* 309:936–938.

19. Rae, B. D., B. M. Long, …, G. D. Price. 2013. Functions, compositions, and evolution of the two types of carboxysomes: polyhedral microcompartments that facilitate CO$_2$ fixation in cyanobacteria and some proteobacteria. *Microbiol. Mol. Biol. Rev.* 77:357–379.

20. Badger, M., D. Hanson, and G. D. Price. 2002. Evolution and diversity of CO$_2$ concentrating mechanisms in cyanobacteria. *Funct. Plant Biol.* 29:161–173.

21. Ort, D. R., S. S. Merchant, …, X. G. Zhu. 2015. Redesigning photosynthesis to sustainably meet global food and bioenergy demand. *Proc. Natl. Acad. Sci. USA.* 112:8529–8536.

22. Zarzycki, J., S. D. Axen, …, C. A. Kerfeld. 2013. Cyanobacterial-based approaches to improving photosynthesis in plants. *J. Exp. Bot.* 64:787–798.

23. Price, G. D., J. J. L. Pengelly, …, J. R. Evans. 2013. The cyanobacterial CCM as a source of genes for improving photosynthetic CO$_2$ fixation in crop species. *J. Exp. Bot.* 64:753–768.

24. Lin, M. T., A. Occhialini, …, M. R. Hanson. 2014. A faster Rubisco with potential to increase photosynthesis in crops. *Nature.* 513:547–550.

25. Frank, S., A. D. Lawrence, …, M. J. Warren. 2013. Bacterial microcompartments moving into a synthetic biological world. *J. Biotechnol.* 163:273–279.

26. Chen, A. H., and P. A. Silver. 2012. Designing biological compartmentalization. *Trends Cell Biol.* 22:662–670.

27. Avalos, J. L., G. R. Fink, and G. Stephanopoulos. 2013. Compartmentalization of metabolic pathways in yeast mitochondria improves the production of branched-chain alcohols. *Nat. Biotechnol.* 31:335–341.

28. Kafri, M., E. Metzl-Raz, …, N. Barkai. 2016. The cost of protein production. *Cell Reports.* 14:22–31.

29. Fridlyand, L., A. Kaplan, and L. Reinhold. 1996. Quantitative evaluation of the role of a putative CO$_2$-scavenging entity in the cyanobacterial CO$_2$-concentrating mechanism. *Biosystems.* 37:229–238.

30. Mangan, N. M., and M. P. Brenner. 2015. Correction: Systems analysis of the CO$_2$ concentrating mechanism in cyanobacteria. *eLife.* 4:e02043.

31. Heinhorst, S., E. B. Williams, …, G. C. Cannon. 2006. Characterization of the carboxysomal carbonic anhydrase CsoSCA from *Halothiobacillus neapolitanus. J. Bacteriol.* 188:8087–8094.

32. Mueller-Cajar, O., and S. M. Whitney. 2008. Evolving improved *Synechococcus Rubisco* functional expression in *Escherichia coli. Biochem. J.* 414:205–214.

33. Tsai, Y., M. R. Sawaya, …, T. O. Yeates. 2007. Structural analysis of CsoS1A and the protein shell of the *Halothiobacillus neapolitanus* carboxysome. *PLoS Biol.* 5:e144.

34. Shively, J. M., F. L. Ball, and B. W. Kline. 1973. Electron microscopy of the carboxysomes (polyhedral bodies) of *Thiobacillus neapolitanus. J. Bacteriol.* 116:1405–1411.

35. Iancu, C. V., H. J. Ding, …, G. J. Jensen. 2007. The structure of isolated *Synechococcus* strain WH8102 carboxysomes as revealed by electron cryotomography. *J. Mol. Biol.* 372:764–773.

36. Shively, J. M., F. Ball, …, R. E. Saunders. 1973. Functional organelles in prokaryotes: polyhedral inclusions (carboxysomes) of *Thiobacillus neapolitanus. Science.* 182:584–586.

37. So, A. K.-C., G. S. Espie, …, G. C. Cannon. 2004. A novel evolutionary lineage of carbonic anhydrase (ε class) is a component of the carboxysome shell. *J. Bacteriol.* 186:623–630.

38. Kim, E. Y., and D. Tullman-Ercek. 2013. Engineering nanoscale protein compartments for synthetic organelles. *Curr. Opin. Biotechnol.* 24:627–632.

39. Cai, F., Z. Dou, …, C. A. Kerfeld. 2015. Advances in understanding carboxysome assembly in *Prochlorococcus* and *Synechococcus* implicate CsoS2 as a critical component. *Life (Basel).* 5:1141–1171.

40. Kaneko, Y., R. Danev, …, H. Nakamoto. 2006. Intact carboxysomes in a cyanobacterial cell visualized by hilbert differential contrast transmission electron microscopy. *J. Bacteriol.* 188:805–808.

41. Iancu, C. V., D. M. Morris, …, G. J. Jensen. 2010. Organization, structure, and assembly of α-carboxysomes determined by electron cryotomography of intact cells. *J. Mol. Biol.* 396:105–117.

42. García-Pérez, A. I., E. A. López-Beltrán, …, S. Cerdán. 1999. Molecular crowding and viscosity as determinants of translational diffusion of metabolites in subcellular organelles. *Arch. Biochem. Biophys.* 362:329–338.

43. Vazquez, A. 2010. Optimal cytoplasmatic density and flux balance model under macromolecular crowding effects. *J. Theor. Biol.* 264:356–359.

44. Dill, K. A., K. Ghosh, and J. D. Schmit. 2011. Physical limits of cells and proteomes. *Proc. Natl. Acad. Sci. USA.* 108:17876–17882.

45. Mugler, A., F. Tostevin, and P. R. ten Wolde. 2013. Spatial partitioning improves the reliability of biochemical signaling. *Proc. Natl. Acad. Sci. USA.* 110:5927–5932.

46. Nunnari, J., and P. Walter. 1996. Regulation of organelle biogenesis. *Cell.* 84:389–394.

47. Smith, J. J., T. W. Brown, …, R. A. Rachubinski. 2000. Regulation of peroxisome size and number by fatty acid β-oxidation in the yeast yarrowia lipolytica. *J. Biol. Chem.* 275:20168–20178.

48. Schrader, M., N. A. Bonekamp, and M. Islinger. 2012. Fission and proliferation of peroxisomes. *Biochim. Biophys. Acta.* 1822:1343–1357.

49. Kiel, J. A. K. W., I. J. van der Klei, …, M. Veenhuis. 2005. Overproduction of a single protein, Pc-Pex11p, results in 2-fold enhanced penicillin production by *Penicillium chrysogenum*. *Fungal Genet. Biol.* 42:154–164.

50. Gomes, L. C., G. Di Benedetto, and L. Scorrano. 2011. During autophagy mitochondria elongate, are spared from degradation and sustain cell viability. *Nat. Cell Biol.* 13:589–598.

51. Liesa, M., and O. S. Shirihai. 2013. Mitochondrial dynamics in the regulation of nutrient utilization and energy expenditure. *Cell Metab.* 17:491–506.

52. Cameron, J. C., S. C. Wilson, …, C. A. Kerfeld. 2013. Biogenesis of a bacterial organelle: the carboxysome assembly pathway. *Cell.* 155:1131–1140.

53. Bondi, A. 1964. van der Waals volumes and radii. *J. Phys. Chem.* 68:441–451.

54. Cheng, S., Y. Liu, …, T. A. Bobik. 2008. Bacterial microcompartments: their properties and paradoxes. *BioEssays.* 30:1084–1095.

55. Bar-Even, A., E. Noor, …, R. Milo. 2011. The moderately efficient enzyme: evolutionary and physicochemical trends shaping enzyme parameters. *Biochemistry.* 50:4402–4410.